Journal of The Electrochemical Society, **157** (2) D119-D125 (2010)
0013-4651/2009/157(2)/D119/7/$28.00 © The Electrochemical Society

Boron Particle Composite Plating with Ni–B Alloy Matrix

Susumu Arai,[a,*,z] Shuji Kasai,[a] and Ikuo Shohji[b]

[a]*Faculty of Engineering, Shinshu University, Nagano 380-8553, Japan*
[b]*Graduate School of Engineering, Gunma University, Gunma 376-8515, Japan*

Ni–B alloy films containing amorphous boron particles (referred to as "Ni–B alloy composite films") were fabricated by electrodeposition and were subsequently subjected to heat-treatment. Their compositions and microstructures were characterized, and their hardness was evaluated. The content of boron particles in the alloy composite films increased with boron particle concentration in the plating baths. In addition, the total boron content in the films increased with decreasing current density, reaching a maximum value of 34.3 atom %. The boron particles were homogeneously distributed in these alloy composite films and exhibited no cohesion. Heat-treatment of the alloy composite films consisting of a Ni–B alloy matrix and the boron particles led to a phase conversion from an inhomogeneous amorphous phase to stable homogeneous crystalline phases, which were similar to those in the Ni–B binary alloy phase diagram. The hardness of the Ni–B alloy 34.3 atom % B composite film was higher than that of a Ni–B alloy film both before and after heat-treatment.
 [DOI: 10.1149/1.3271099]

Manuscript submitted July 6, 2009; revised manuscript received November 11, 2009. Published December 29, 2009.

Ni–B alloy films are attractive for industrial applications because they possess several desirable properties, including high hardness and wear resistance. To date, such films have mainly been deposited by electroless plating methods,[1-11] and their applications have also been studied.[12-18] However, very few studies have been undertaken on Ni–B alloy films produced by electroplating methods.[19-21] Most reports discuss alloy films with a boron content of under 25 atom %, which have the stable phases of Ni and Ni_3B according to the Ni–B binary phase diagram. However, the phase diagram also indicates that Ni_2B and other crystalline phases are stable when the boron content of Ni–B alloys exceeds 25 atom %. A comparison of the microstructure and characteristics of Ni–B alloy films having boron contents above and below 25 atom % is interesting from both an academic and a practical viewpoint. We initially attempted to fabricate Ni–B alloy films using a conventional electroplating method. However, the maximum boron content that could be achieved by this method was less than 25 atom %. We have already reported that Ni–P alloy films containing over 25 atom % phosphorus could be obtained using a unique technique, which involves the formation of a composite film of a Ni–P alloy and phosphorus particles and a subsequent heat-treatment.[22]

In the present study, to fabricate Ni–B alloy films with boron contents greater than 25 atom %, we used a similar technique, producing composite films of a Ni–B alloy and boron particles and then subjecting them to heat-treatments. Furthermore, we analyzed the microstructure and hardness of the alloy composite films both before and after heat-treatment.

Experimental

The compositions of the plating baths used in the present study are shown in Table I. The baths were based on the Watts bath, and a Ni–B alloy and a Ni–B composite bath were prepared for comparison. Trimethylamine borane was used as a boron source for the Ni–B alloy plating bath,[19] and boron particles were used as a boron source for the Ni–B composite plating bath. Both sources were used for the Ni–B alloy composite plating bath. Amorphous boron particles (Rare Metallic Co., Ltd.) with an 800 nm average diameter were used in this study. An electrolytic cell (model I, Yamamoto-Ms Co., Ltd.) with internal dimensions of $65 \times 65 \times 95$ mm was employed for electrodeposition. The volume of the plating bath was 250 cm^3. Pure copper plates (C1020P) and stainless steel plates (SUS304), both having exposed surface areas of 10 cm^2 (3×3.3 cm^2), were used as substrates. A pure nickel plate was used as the anode. Plating was performed under galvanostatic conditions. The Ni–B alloy plating and the Ni–B alloy composite plating were carried out at 45°C with aeration. The Ni–B composite plating was conducted at 25°C with aeration. The compositions of the deposited films were measured using an inductively coupled plasma emission spectrometer (ICPS-7500, Shimadzu Seisakusho Co.). Before the measurement, the deposited films were dissolved in nitric acid, resulting in nickel ions (Ni^{2+}) and boric acid ions (BO_3^{3-}). Boron concentration was determined as the boric acid ion concentration. The deposited films were heat-treated in vacuum using an IR heating furnace. Their phase structures were analyzed using an X-ray diffractometer (XRD, XRD-6000, Shimadzu Seisakusho Co.). Surface morphologies and cross-sectional textures were observed using a field-emission scanning electron microscope (SEM, JSM-7000F, JEOL). A mapping analysis of the cross sections of the deposits was performed using an electron probe X-ray microanalyzer (EPMA, EPMA-1610, Shimadzu Seisakusho Co.). A cross-section polisher (SM-09010, JEOL) was used to prepare cross-sectional samples for observation. Hardness testing of the deposited films was performed using a micro-Vickers hardness tester (DUH-201, Shimadzu Seisakusho Co.).

Results and Discussion

Figure 1 shows the relationship between the concentration of boron particles in the plating bath and the boron content in the electrodeposited films. The applied current density was 1 A dm^{-2}. The boron content in the films includes the boron component of the Ni–B alloy matrix and the boron particles in the films. The Ni–B alloy film electrodeposited from the bath without boron particles contained 6.4 atom % boron. The boron content of the deposited films increased as the concentration of boron particles in the plating bath increased, reaching a maximum value of 22.5 atom %. Homogeneous composite films could not be fabricated when the boron particle concentration in the plating bath exceeded 100 g dm^{-3}.

Figure 2 shows surface and cross-sectional SEM images of films with various boron contents. Figure 2a and d shows the surface and the cross section of a Ni–6.4 atom % B alloy film. The film has a smooth surface morphology and a homogeneous microstructure. Figure 2b, e, c, and f shows the surfaces and cross sections of the Ni–17.1 atom % B alloy composite film and the Ni–22.5 atom % B alloy composite film, respectively. Boron particles are homogeneously distributed in the films without any cohesion. The quantity of boron particles in the films evidently increased with the overall boron content of the films, which is related to the boron particle concentration in the plating baths. Therefore, the increase in the boron content in the films in Fig. 1 is considered to be caused mainly by the increase in the number of boron particles in the films.

Figure 3 shows the effect of current density on the boron content in the electrodeposited films. The boron particle concentration in the alloy composite bath was 100 g dm^{-3}. The boron content in the Ni–B alloy films increased with decreasing current density. This

* Electrochemical Society Active Member.
z E-mail: araisun@shinshu-u.ac.jp

Table I. Compositions of various plating baths.

Chemicals	Ni–B alloy bath (M)	Ni–B composite bath	Ni–B alloy composite bath
$NiSO_4 \cdot 6H_2O$	1	1 M	1 M
$NiCl_2 \cdot 6H_2O$	0.2	0.2 M	0.2 M
H_3BO_3	0.5	0.5 M	0.5 M
Trimethylamine borane	0.1		0.1 M
Saccharin sodium dehydrate		0.1 M	
2-Butyne-1,4-diol		2.5×10^{-3} M	
Boron particle		100 g dm^{-3}	30–100 g dm^{-3}

tendency is similar to that reported by Krishnaveni et al. using the dimethylamine borane as a boron source.[20] The boron content in the Ni–B composite films slightly increased with decreasing current density. For the Ni–B alloy composite films, the boron content also increased with decreasing current density, reaching a maximum value of 34.3 atom %, which is obviously higher than 25 atom %. The boron content of the Ni–B alloy composite films at any given current density seems to be the sum of that of the Ni–B alloy film and the Ni–B composite film at the same current density. This suggests that the boron component of the Ni–B alloy matrix and the boron in the particles are independent of each other.

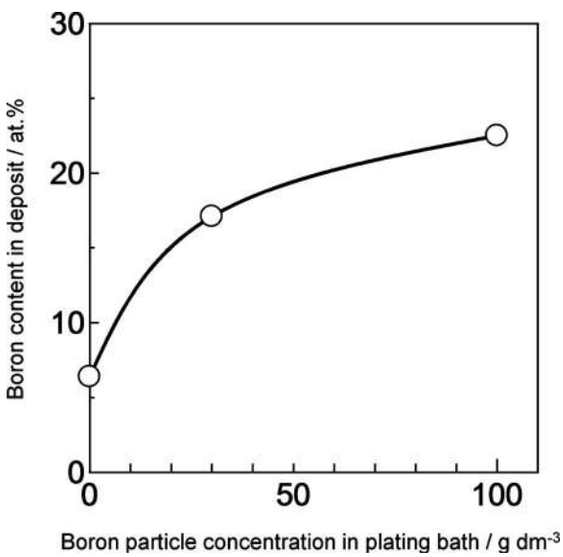

Figure 1. Relationship between the boron particle concentration in the plating bath and the boron content in the electrodeposited film. The current density is 1 A dm^{-2}.

Figure 4 shows surface and cross-sectional SEM images of the Ni–B alloy composite films electrodeposited under various current densities. A uniform distribution of boron particles was found for every alloy composition, with no evidence of cohesion. Whereas the boron content of the film electrodeposited at 0.5 A dm^{-2} (Ni–34.3 atom % B) is clearly higher than that of the film electrodeposited at 1 A dm^{-2} (Ni–22.5 atom % B), the difference in the amount of boron particles in those films is not so obvious. Therefore, the difference in the overall boron content is thought to be due to differing amounts of boron in the Ni–B alloy matrix. Figure 5 shows XRD patterns of the Ni–B alloy composite films. For each film, a broad peak assigned to Ni appears at around 44°, indicating that the alloy composite films have low crystallinity or an amorphous structure. In particular, the peak for the Ni–34.3 atom % B alloy composite film is extremely broad. This is thought to be largely due to the increase in the boron content in the Ni–B alloy matrix and supports the idea that the difference in the overall boron content between the Ni–34.3 atom % and the Ni–22.5 atom % B alloy composite film is mainly due to the difference in the boron content in the Ni–B alloy matrix.

Figure 6 shows surface SEM images of the Ni–34.3 atom % B alloy composite film following heat-treatment at various temperatures. No significant defects such as cracks could be observed in any of the films, and morphological changes did not occur up to 400°C. However, the size of the boron particles became smaller above 500°C possibly due to the accelerated interdiffusion between the boron particles and the Ni–B alloy matrix. Figure 7 shows cross-sectional SEM images of the Ni–34.3 atom % B alloy composite film following heat-treatments at various temperatures. No cracks are observed in any of the films, and no changes in the microstructure are seen up to 400°C. Above 500°C, the number of boron particles appears to decrease. Figure 8 shows magnified images of

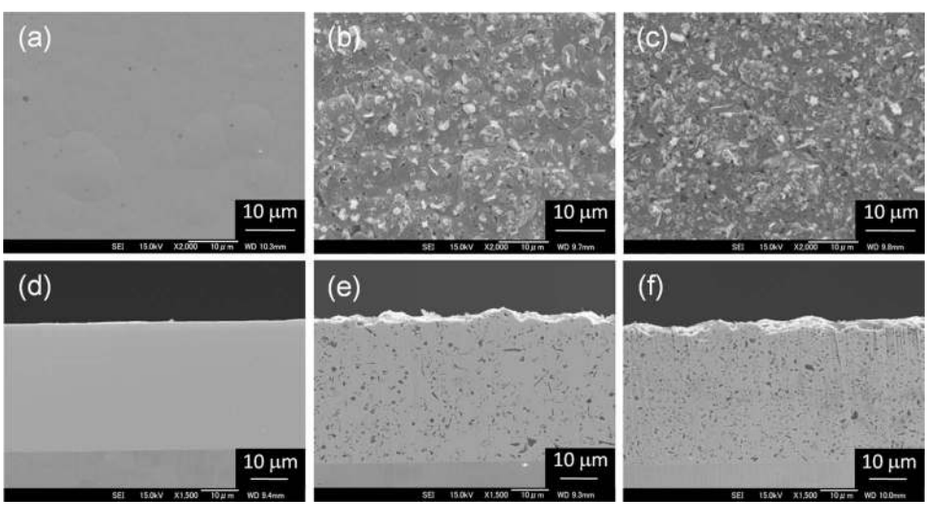

Figure 2. Surface and cross-sectional SEM images of electrodeposited films with various boron contents. (a)–(c) show surface SEM images of the Ni–6.4 atom % B alloy film, the Ni–17.1 atom % B alloy composite film, and the Ni–22.5 atom % B alloy composite film, respectively. (d)–(f) show the cross-sectional SEM images of (a)–(c), respectively.

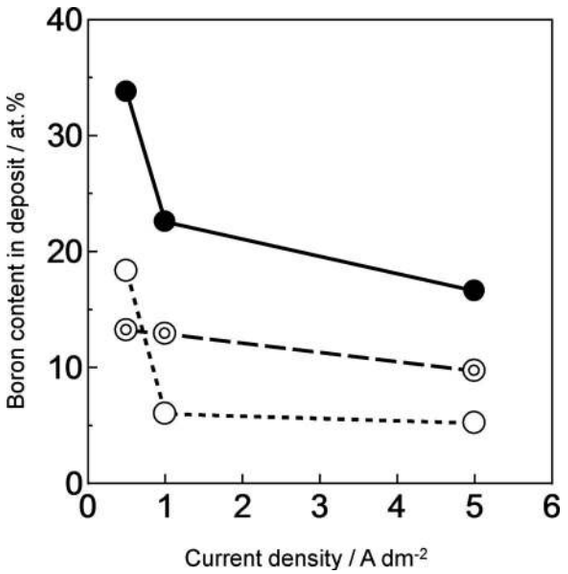

Figure 3. Effect of current density on the boron content in films electrodeposited in different plating baths. White circles with short dashed lines: Ni–B alloy plating bath; double circles with dashed lines: Ni–B composite plating bath; and black circles with solid lines: Ni–B alloy composite plating bath (the boron particle concentration is 100 g dm^{-3}).

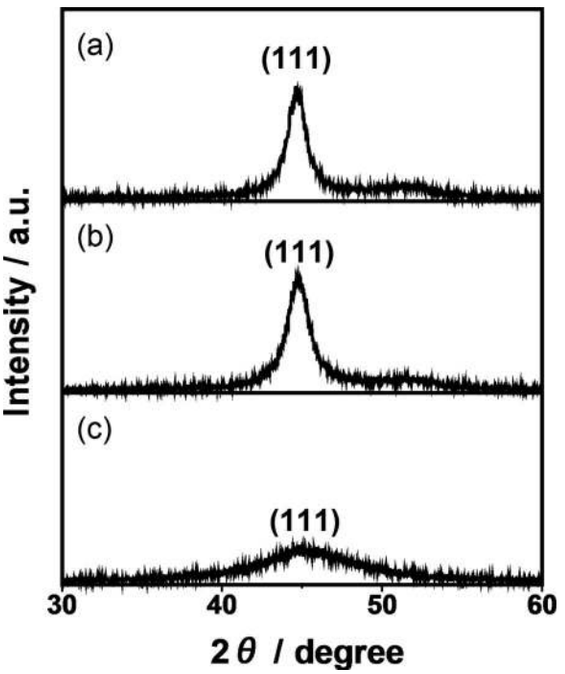

Figure 5. XRD patterns of (a) the Ni–16.6 atom % B alloy composite film, (b) the Ni–22.5 atom % B alloy composite film, and (c) the Ni–34.3 atom % B alloy composite film.

the regions shown in Fig. 7. Again, no change in the microstructure is seen up to 400°C. However, above 500°C, the density of boron particles begins to decrease, and many voids start to appear. These voids are most likely the result of the Kirkendall effect due to the enhanced interdiffusion between the boron particles and the Ni–B alloy matrix. The diffusion velocity of boron from the boron particles to the Ni–B alloy matrix may be higher than that of nickel from the Ni–B alloy matrix to the boron particles, leading to void formation.

To clarify the interdiffusion behavior of the boron particles and the Ni–B alloy matrix, EPMA analysis was carried out. Figure 9 shows EPMA elemental mappings of cross sections of the Ni–34.3 atom % B alloy composite films following heat-treatment at different temperatures. Before heat-treatment, it is evident from the boron mapping that boron particles undoubtedly exist in the film. No obvious difference in the boron distribution is seen following heat-treatment at 400°C. However, the amount of boron particles obviously decreases at 500°C, and a relatively homogeneous boron distribution can be seen at 600°C. These results strongly suggest that the interdiffusion of boron and nickel between the boron particles and the Ni–B alloy matrix is highly accelerated over 500°C. It is also evident that a Ni–B alloy film with a homogeneous microstructure can be formed from a Ni–B alloy composite film by heat-treatment.

Figure 10 shows XRD patterns of the Ni–34.3 atom % B alloy composite film following heat-treatment at various temperatures. The broad peak previously assigned to nickel becomes sharper at 200°C, and the sharp peaks assigned to nickel and Ni_3B appear at 300 and 400°C. Using differential scanning calorimetry and XRD, Lee et al. determined that the phase transition in Ni–B alloy films from a metastable amorphous phase to a stable crystalline phase, i.e., the precipitation of the Ni_3B phase, occurred at different temperatures depending on the boron content in the films, and precipi-

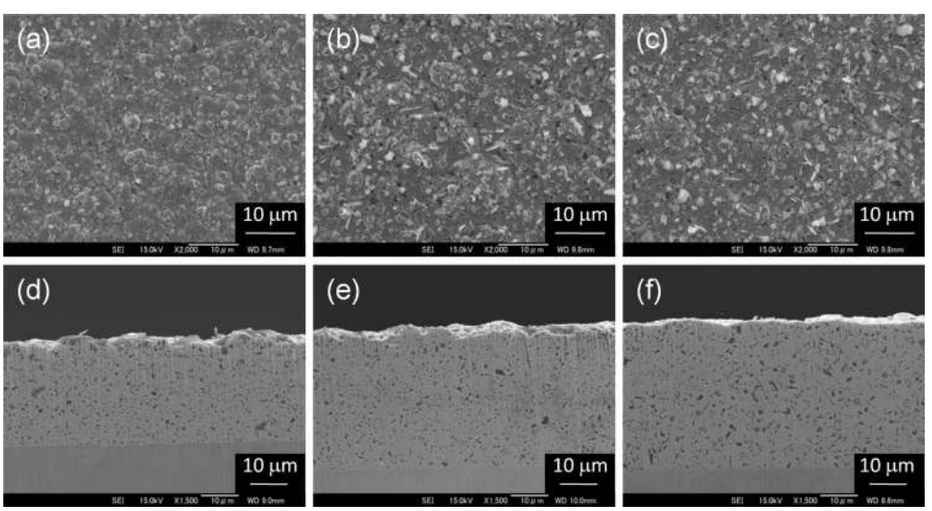

Figure 4. Surface and cross-sectional SEM images of films electrodeposited under various current densities. (a)–(c) show the surface SEM images of the Ni–16.6 atom % B alloy composite film, the Ni–22.5 atom % B alloy composite film, and the Ni–34.3 atom % B alloy composite film, respectively. (d)–(f) show the cross-sectional SEM images of (a)–(c), respectively.

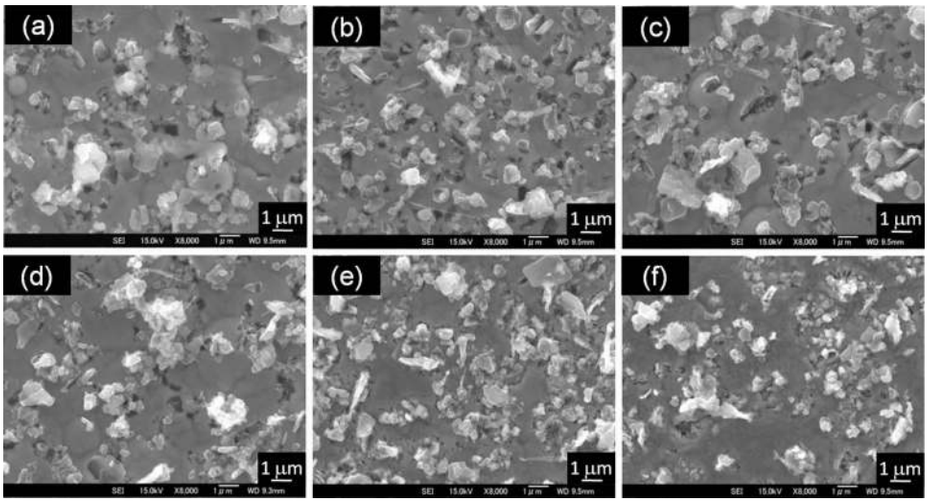

Figure 6. Surface SEM images of the Ni–34.3 atom % B alloy composite film heat-treated at various temperatures: (a) Before heat-treatment, (b) 200, (c) 300, (d) 400, (e) 500, and (f) 600°C.

tation of the Ni_3B phase was observed at 300°C for boron contents above 9 atom %.[19] Because the boron content in the Ni–B alloy matrix of the Ni–34.3 atom % B alloy composite film is considered to be at least more than 9 atom % in Fig. 3-5, the appearance of the peaks assigned to the Ni_3B phase at 300 and 400°C is almost certainly due to the phase transition of the Ni–B alloy matrix. On the contrary, above 500°C, the only sharp peaks observed are those assigned to Ni_3B and Ni_2B. Although these peaks often overlap and make the assignment difficult, especially for Ni_2B, clear peaks due to Ni_2B do appear at around 25 and 36°. According to the Ni–B

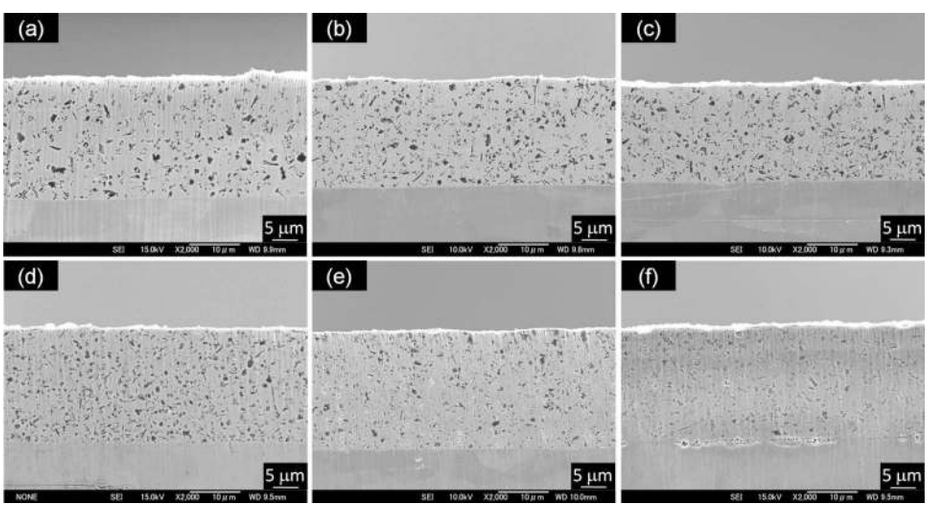

Figure 7. Cross-sectional SEM images of the Ni–34.3 atom % B alloy composite film heat-treated under various temperatures: (a) Before heat-treatment, (b) 200, (c) 300, (d) 400, (e) 500, and (f) 600°C.

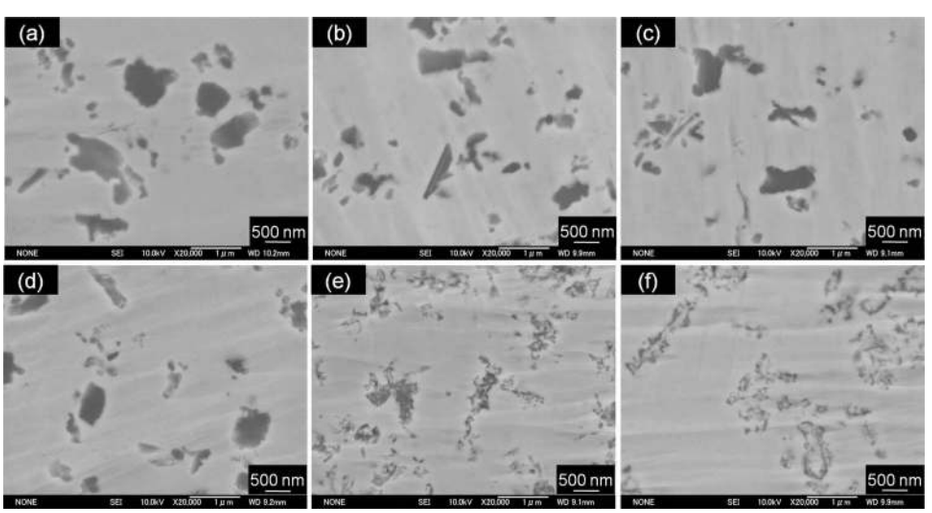

Figure 8. Enlarged images of the regions represented in Fig. 7: (a) Before heat-treatment, (b) 200, (c) 300, (d) 400, (e) 500, and (f) 600°C.

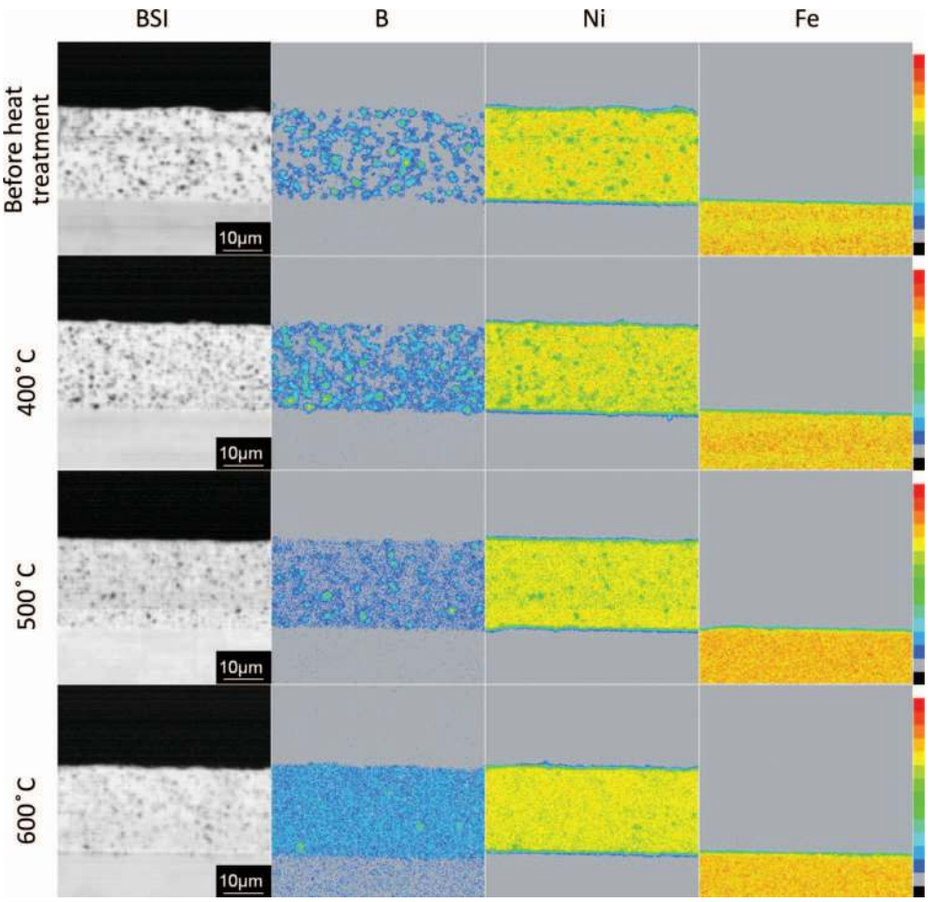

Figure 9. EPMA mapping analysis of cross sections of the Ni–34.3 atom % B alloy composite film heat-treated at various temperatures.

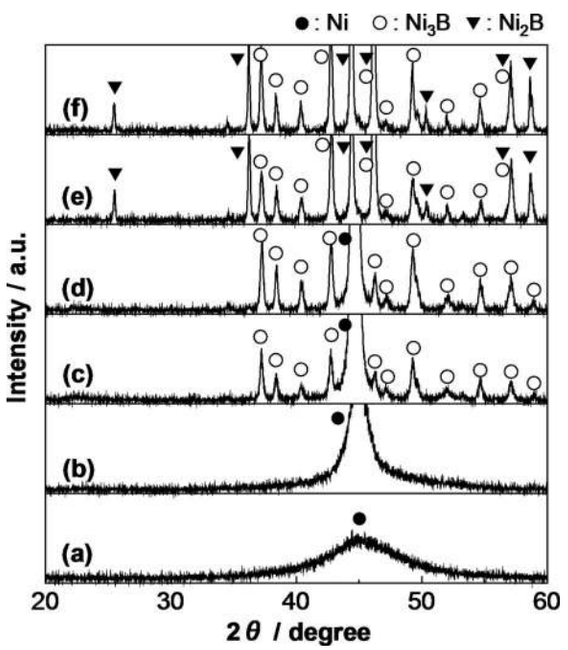

Figure 10. XRD patterns of the Ni–34.3 atom % B alloy composite film heat-treated at various temperatures: (a) Before heat-treatment, (b) 200, (c) 300, (d) 400, (e) 500, and (f) 600°C.

binary alloy phase diagram (Fig. 11),[23] at temperatures above 700°C, the Ni_2B and o-Ni_4B_3 phases are the stable phases for boron content from 33.3 to 41.4 atom %, whereas the Ni_3B and Ni_2B phases are the stable phases for boron content from 25.0 to 33.3 atom %. If the stable phases at room temperature are assumed to be the same as those above 700°C, the Ni–34.3 atom % B alloy composite film heat-treated at 600°C would be expected to consist of the Ni_2B and o-Ni_4B_3 phases. However, as shown in Fig. 10, it is actually composed of the Ni_3B and Ni_2B phases. One possible explanation may be that the interdiffusion between the boron particles and the Ni–B alloy matrix does not reach completion, and the composition of the Ni–B alloy matrix does not exceed 33.3 atom %. A few boron particles remain in the film, as seen in Fig. 9. Furthermore, some of the boron may have diffused into the iron substrate, causing a decrease in the boron content, resulting in the Ni_3B and Ni_2B phases.

Figure 12 shows the effects of the heat-treatment temperature on the hardness of the Ni–34.3 atom % B alloy composite film. The result for the Ni–6.4 atom % B alloy film is also shown for comparison. The hardness increased with increasing heat-treatment temperature, reaching a maximum value of 1250 HV at 300°C before decreasing again, and was higher than that of the Ni–6.4 atom % B alloy film over the full temperature range studied. For temperatures up to 200°C, the main contribution to the increased hardness of the Ni–B alloy composite film may be the dispersion hardening of boron particles. Between 300 and 400°C, both the dispersion hardening of boron particles and the precipitation hardening of the Ni_3B phase are likely to be the main causes of the higher hardness. The hardness of the Ni–6.4 atom % B alloy film rapidly decreases with increasing heat-treatment temperature over 300°C, which is almost the same result reported by Lee et al.[19] The strength (or hardness) of polycrystalline materials is expected to increase with decreasing grain

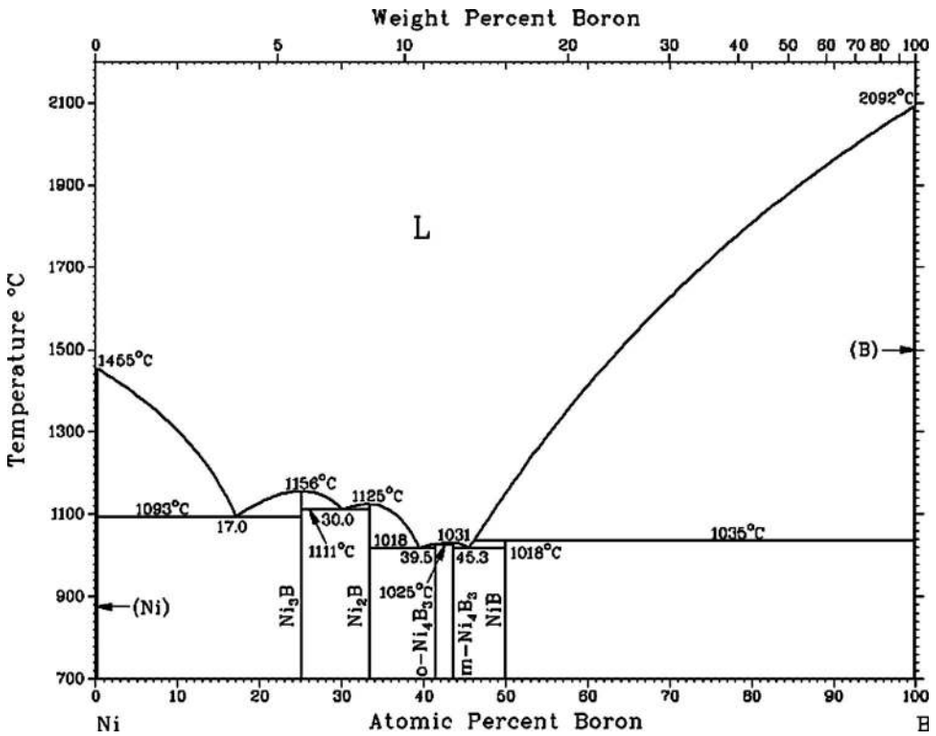

Figure 11. Ni–B binary alloy phase diagram.[23]

size based on the classical Hall–Petch (H–P) relationship, $\sigma = \sigma_0 + k_h d^n$, where d is the grain size, σ is the 0.2% yield strength (or hardness), σ_0 is the lattice friction stress to move individual dislocations (or the hardness of a single-crystal specimen, $d \rightarrow \infty$), n is the grain size exponent (normally $-1/2$), and k_h is a constant called the H–P intensity parameter.[24] The Ni–6.4 atom % B alloy film must consist of the nickel and the Ni_3B phases.[19] The rapid decrease in hardness may be the result of an increase in the grain size of the nickel phase owing to recrystallization. However, the hardness of the Ni–34.3 atom % B alloy composite film did not decrease rapidly at 500 and 600°C. Because dispersion hardening of boron particles is not expected over 500°C, as shown in Fig. 8 and 9, the difference in hardness between the alloy composite film and the alloy film might be related to the difference in the intrinsic hardness of the crystalline phases. The hardness of Ni_3B and Ni_2B is reported to be 900 and 1500 HV, respectively.[25] Torun and Celikyürek reported that Ni–B alloy layers consisting of the Ni_3B and Ni_2B phases could be prepared by boriding pure nickel, and the alloy layer exhibited a high hardness of 1300 ± 15 HV.[26] Therefore, the higher hardness of the Ni–B alloy composite film heat-treated above 500°C may be caused by the intrinsically high hardness of the Ni_3B phase and the Ni_2B phases.

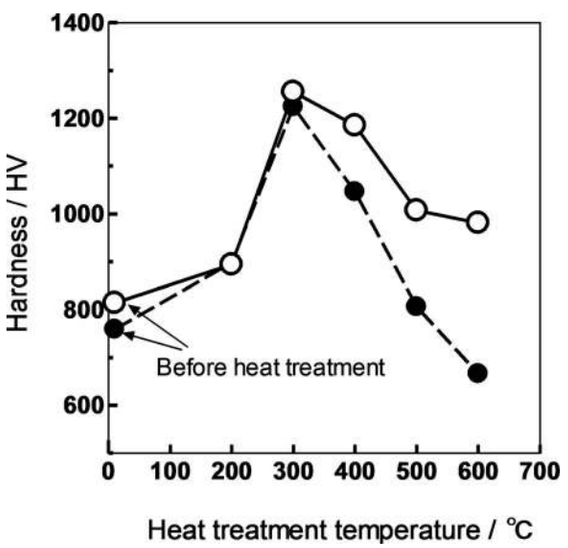

Figure 12. Effect of heat-treatment temperature on the hardness of the films. Black circles with dashed lines: Ni–6.4 atom % B alloy film; white circles with solid lines: Ni–34.3 atom % B alloy composite film.

Conclusions

Ni–B alloy films containing boron particles (Ni–B alloy composite films) produced by electrodeposition were subjected to heat-treatment, and their microstructure and hardness were characterized. The main conclusions are as follows

1. The boron content in the alloy composite films increased with increasing boron particle concentration in the plating bath, reaching a maximum value of 34.3 atom %.
2. The boron particles were uniformly distributed in the Ni–B alloy composite films.
3. When the Ni–34.3 atom % B alloy composite film was heat-treated above 500°C, the microstructure became homogeneous due to interdiffusion between boron particles and the Ni–B alloy matrix.
4. Both before and after heat-treatment, the hardness of the Ni–34.3 atom % B alloy composite film was higher than that of the Ni–6.4 atom % B alloy film.

Shinshu University assisted in meeting the publication costs of this article.

References

1. W. Goldie, *Metallic Coating of Plastics*, Vol. 1, Electrochemical Publications, London (1968).
2. N. Hedgecock, P. Tung, and M. Schlesinger, *J. Electrochem. Soc.*, **122**, 866 (1975).
3. A. Chiba, H. Haijima, and K. Kobayashi, *Surf. Coat. Technol.*, **169–170**, 104

(2003).
4. T. S. N. Sankara Narayanan and S. K. Seshadri, *J. Alloys Compd.*, **365**, 197 (2004).
5. C. T. Dervos, J. Novakovic, and P. Vassiliou, *Mater. Lett.*, **58**, 619 (2004).
6. Q. Rao, G. Bi, Q. Lu, H. Wang, and X. Fan, *Appl. Surf. Sci.*, **240**, 28 (2005).
7. K. Krishnaveni, T. S. N. Sankara Nayayanan, and S. K. Seshadri, *Surf. Coat. Technol.*, **190**, 115 (2005).
8. I. Baskaran, R. Sakthi Kumar, T. S. N. Sankara Narayanan, and A. Stephen, *Surf. Coat. Technol.*, **200**, 6888 (2006).
9. W. X. Zhang, Z. H. Jiang, G. Y. Li, Q. Jiang, and J. S. Lian, *Appl. Surf. Sci.*, **254**, 4949 (2008).
10. B. Oraon, G. Majumdar, and B. Ghosh, *Mater. Des.*, **28**, 2138 (2007).
11. B. Oraon, G. Majumdar, and B. Ghosh, *Mater. Des.*, **29**, 1412 (2008).
12. B. K. Singh, A. Chatterjee, A. N. Daw, and R. N. Mitra, *J. Electrochem. Soc.*, **136**, 785 (1989).
13. M. Velez, H. Quinones, A. R. Di Giampaolo, J. Lira, and I. C. Grigorescu, *Int. J. Refract. Met. Hard Mater.*, **17**, 99 (1999).
14. D. Xue and J. F. Deng, *Mater. Lett.*, **47**, 271 (2001).
15. T. Tsunoda, T. Okabe, and H. Honma, *J. Electrochem. Soc.*, **151**, C610 (2004).
16. X. Li, X. Han, Y. Tan, and P. Xu, *J. Alloys Compd.*, **464**, 352 (2008).
17. J. W. Yoon, J. M. Koo, J. W. Kim, S. S. Ha, B. I. Noh, C. Y. Lee, J. H. Park, C. C. Shur, and S. B. Jung, *J. Alloys Compd.*, **466**, 73 (2008).
18. H. Zhou, Q. Yu, Q. Peng, H. Wang, J. Chen, and Y. Kuang, *Mater. Lett.*, **110**, 434 (2008).
19. K. H. Lee, D. Chang, and S. C. Kwon, *Electrochim. Acta*, **50**, 4538 (2005).
20. K. Krishnaveni, T. S. N. Sankara Narayanan, and S. K. Seshadri, *Mater. Chem. Phys.*, **99**, 300 (2006).
21. K. Krishnaveni, T. S. N. Sankara Narayanan, and S. K. Seshadri, *J. Alloys Compd.*, **480**, 765 (2009).
22. Y. Suzuki, S. Arai, I. Shohji, and E. Kobayashi, *J. Electrochem. Soc.*, **156**, D283 (2009).
23. The Materials Information Society, *Binary Alloy Phase Diagrams*, 2nd ed., ASM International, Materials Park, OH (1996).
24. E. O. Hall, *Proc. Phys. Soc. London, Sect. B*, **64**, 747 (1951).
25. İ. Celikyürek, Ph.D. Thesis, Eskisehir Osmangazi University, Turkey (2006).
26. O. Torun and İ. Celikyürek, *Mater. Des.*, **30**, 1830 (2009).